Journal of Materials Chemistry A

PAPER

View Article Online
View Journal | View Issue

Cite this: J. Mater. Chem. A, 2019, 7, 2087

Selenization of $CuInS_2$ by rapid thermal processing – an alternative approach to induce a band gap grading in chalcopyrite thin-film solar cell absorbers?†

Roberto Félix,*[a] Alfons Weber,[a] Ole Zander,[a] Humberto Rodriguez-Álvarez,[a] Björn-Arvid Schubert,[a] Joachim Klaer,[a] Regan G. Wilks,[ab] Hans-Werner Schock,[a] Roland Mainz[a] and Marcus Bär[abcd]

Received 9th November 2018
Accepted 22nd December 2018

DOI: 10.1039/c8ta10823d

rsc.li/materials-a

A treatment of $CuInS_2$ (CIS) based on rapid thermal processing (RTP) selenization is developed, aiming at tuning the absorber's band gap grading using the [Se]/([S] + [Se]) composition. X-ray photoelectron spectroscopy and X-ray fluorescence analysis measurements of RTP-treated CIS samples (with the used set of RTP-parameter ranges) show a greater treatment effect at the surface of the sample compared to the bulk. A tuning of the [Cu] : [In] : ([S] + [Se]) surface composition from a Cu-poor 1 : 3 : 5 to a 1 : 1 : 2 stoichiometry is also observed in RTP-treated CIS absorbers with lower to higher surface Se contents, respectively. Ultraviolet photoelectron spectroscopy measurements show a shift in valence band maximum toward the Fermi level, E_F, in higher surface Se content samples [from (−0.88 ± 0.1) to (−0.51 ± 0.1) eV], as expected for a reduction of the (surface) band gap produced by exchanging S with Se. Ultraviolet-visible spectrophotometry reveals a reduction in the optical (bulk) band gap of samples with greater Se incorporation [from (1.47 ± 0.05) to (1.08 ± 0.05) eV], allowing for a working window for optimization purposes.

Introduction

The chalcopyrite $Cu(In_{1-x}Ga_x)(S_ySe_{1-y})_2$ (CIGSSe) alloy system is one of the most promising absorber materials used in thin-film solar cell devices, which are typically stacked in the following p–n heterojunction configuration (from top to bottom): n^+/i-type ZnO window bi-layer/n-type buffer layer/p-type chalcopyrite absorber/Mo-coated soda-lime glass (SLG). Many laboratories have already reported chalcopyrite-based thin-film solar cells with power conversion efficiencies, η, surpassing 20% on the laboratory-scale[1–8] (record η: 22.9%[1]). One of the main features of the CIGSSe alloy system is that by changing the elemental x = [Ga]/([In] + [Ga]) and y = [S]/([S] + [Se]) composition of the absorber, its optical (*i.e.*, bulk) band gap energy (E_g) can be varied between 1.04 eV (for $x = 0$, $y = 0 \rightarrow CuInSe_2$, CISe) and 2.53 eV (for $x = 1$, $y = 1 \rightarrow CuGaS_2$, CGS).[9] The possibility of tuning the E_g of an absorber to match the theoretical optimum absorber E_g for terrestrial solar energy conversion (*i.e.*, E_g ~1.4 eV (ref. 10 and 11)) or implementing a beneficial band gap grading[12] is one of the key parameters that are optimized to push the performance of chalcopyrite solar devices closer to the theoretical maximum efficiency for a single p–n junction solar cell, *ca.* 30%.[10,11] The highest efficiencies[1–8] reported for chalcopyrite-based solar cells are based on $Cu(In_{1-x}Ga_x)Se_2$ (CIGSe) absorbers with an average composition of $x \approx 0.3$ and $y = 0$, resulting in a E_g of ≈1.2 eV; so it comes as no surprise that varying the elemental grading x is the parameter of choice in band gap grading efforts of chalcopyrite absorbers. However, a reproducible control of the [Ga]/([In] + [Ga]) throughout the absorber layer profile continues to be a challenge.[13–19] Finding a straightforward approach to control the [Se]/([S] + [Se]) profile distribution of chalcopyrite absorbers would be an effective alternative route to produce band gap grading configurations.

In this contribution, the results of selenization treatments of $CuInS_2$ (CIS, $E_g = 1.54$ eV (ref. 20)) absorbers by a rapid thermal process (RTP) in Se vapor are presented and the effect on the chemical and electronic surface and bulk properties monitored. The feasibility of tuning the absorber's band gap grading using the [Se]/([S] + [Se]) composition by extending the effect of the selenization treatment into the bulk of the absorber layer, as illustrated in Fig. 1, are here discussed. The influence of the

[a]Renewable Energy, Helmholtz-Zentrum Berlin für Materialien und Energie GmbH, Hahn-Meitner-Platz 1, D-14109 Berlin, Germany. E-mail: roberto.felix_duarte@helmholtz-berlin.de

[b]Energy Materials In-Situ Laboratory Berlin (EMIL), Helmholtz-Zentrum Berlin für Materialien und Energie GmbH, Albert-Einstein-Straße 15, D-12489 Berlin, Germany

[c]Helmholtz-Institute Erlangen-Nürnberg for Renewable Energy, Forschungszentrum Jülich, Egerlandstr. 3, D-91058 Erlangen, Germany

[d]Department of Chemistry and Pharmacy, Friedrich-Alexander-Universität Erlangen-Nürnberg, Egerlandstr. 3, D-91058 Erlangen, Germany

† Electronic supplementary information (ESI) available. See DOI: 10.1039/c8ta10823d

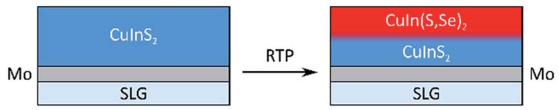

Fig. 1 Targeted composition modification of CIS absorbers.

selenization treatment (*e.g.*, RTP temperature, RTP duration, and Se amount) on surface and bulk properties is determined by a non-destructive depth-resolved chemical and electronic structure analysis, using a suite of complementary spectroscopic techniques.

Experimental

Materials and methods

CIS absorbers of ~2 μm thickness were prepared by direct current (DC) magnetron sputtering *via* successive deposition of Cu and In on Mo-coated SLG back contacts followed by RTP sulfurization.[21] Prior to the selenization treatment, the CIS samples were treated with a KCN etching process to remove Cu_xS binary phases from the absorber surface.[22]

The RTP selenization treatments were carried out inside a graphite ring cylinder sealed by two quartz discs.[23] (This assembly is referred to as a graphite box.) The baseline pressure of the RTP-chamber was $\sim 5 \times 10^{-4}$ mbar. During a 1 min heating ramp step, the temperature inside the graphite box reaches the selected RTP-temperature by means of two sets of lamps positioned at the top and bottom of the graphite box that act as heating sources. Once the selected RTP-temperature is reached, it is kept for the duration of the treatment. The selenization is conducted in elemental Se vapor. Table 1 summarizes the parameters used in the RTP treatments and the resulting samples.

When samples were transported for measurement purposes outside ultra-high vacuum (UHV), they were sealed in N_2 (in order to minimize their exposure to air). During bulk-sensitive characterization, samples were exposed to ambient conditions. Therefore, these measurements were conducted only after the more surface-sensitive spectroscopic techniques were performed.

Chemical and electronic surface characterization

The chemical and electronic *surface* structures of the treated CIS absorbers were studied using X-ray photoelectron (XPS), X-ray-excited Auger electron (XAES) and ultraviolet photoelectron (UPS) spectroscopies.

Table 1 List of samples and RTP treatment parameters

Sample	Se amount (mg)	Duration (min)	Temperature (°C)
CIS	—	—	—
i	—	30	500
ii	5	5	300
iii	5	5	400
iv	5	5	500
v	5	30	470
vi	5	30	500
vii	5	30	530

The XPS and XAES measurements were carried out employing a SPECS PHOIBOS 150MCD electron analyzer and (non-monochromatized) Mg K_α and Al K_α excitation energies. The energy scale for all these measurements was calibrated in accordance with ref. 24. The elemental surface composition of the absorber was derived by evaluating the intensity of the Cu $2p_{3(1)/2}$, In $3d_{3/2}$, S 2s, and Se 3s core level peaks, as determined by curve fit analysis of the spectra conducted with the Fityk software.[25] Voigt profile functions, along with linear backgrounds, were used for these fits. The peak intensities of the XPS core levels were corrected to account for differences in inelastic mean free path (λ),[26,27] photoionization cross section (σ),[28] and the transmission function of the electron analyzer (T).[29] The S 2s/Se 3s lines were also used to assess the impact of the RTP-treatment on the surface [Se]/([S] + [Se]) composition of the samples. Because of the energetic proximity of these two photoemission lines, intensity changes associated with differences in λ and T are negligible. This arrangement considerably simplifies the analysis because the core level intensities need to only be corrected for their different σ.[28] The analysis of modified Auger parameters ($\alpha^* = BE_{XPS} + KE_{XAES}$, where BE_{XPS} and KE_{XAES} are the binding and kinetic energies of the evaluated XPS and XAES lines, respectively)[24,30] of Cu-, In- and Se-related emission lines was used to determine changes in the chemical structure of the RTP-treated samples. The modified Se α^*, Cu α^*, and In α^* values were derived by using the Se $3d_{5/2}$ XPS core level and the Se $L_3M_{45}N_{45}$ (LMM) XAES line, the Cu $2p_{3(1)/2}$ XPS core level and the Cu LMM XAES line, and the In $3d_{3/2}$ XPS core level and the In $M_4N_{45}N_{45}$ (MNN) XAES line, respectively. The Se $3d_{5/2}$ core level is chosen for this chemical environment evaluation (instead of Se 3s) for the following reasons: (i) the full width at half maximum (FWHM) value of the Se 3d peaks (1.2 eV), as determined by the curve fit analysis of the peaks, is significantly smaller than the FWHM value of the Se 3s peaks (3 eV). Therefore, the Se 3d XPS line is more sensitive to detect changes in peak shape associated with chemical speciation. (ii) The Se $3d_{5/2}$ + Se $L_3M_{45}M_{45}$ modified Auger parameter is the most prevalent modified Se α^* that can be found in literature.[24,30]

Surface-sensitive UPS measurements were conducted using He I excitation. The position of the valence band maximum (VBM) with respect to the Fermi level (E_F) was determined by linear approximation of the leading edge of the UPS spectra.[31–36] The kinetic energy (KE) of photoelectrons derived from the VBM edge is ~20 eV. Based on the "universal curve" of electron λ as a function of KE,[37] the exponentially decreasing information depth (ID, taken as $3 \times \lambda$) of this technique is estimated to be ~1 nm. The energy scale of UPS spectra is referenced to the measured E_F level of a sputter-cleaned Au foil.

Bulk elemental analysis

Bulk elemental analysis was conducted *via* X-ray fluorescence analysis (XRF). A wavelength-dispersive XRF spectrometer (Rigaku WD-XRF ZSX Primus II) with an end-window-type Rh-target X-ray source was used for the XRF measurements.[38] A

LiF(200) crystal setup was used for wavelength dispersion of the emitted fluorescent X-ray lines, along with a P10-gas flow proportional counter (PC) and a scintillation counter (SC) detector systems. The Cu K_α, In K_α, S K_α and Se K_α lines of the samples were analyzed. Based on the effective attenuation length of these emission lines in the chalcopyrite,[39] the information depth of this technique is estimated to be several tens of μm, an order of magnitude higher than the thickness of the studied absorber layers.[21]

The evolution of Se incorporation into the film was studied in real-time by synchrotron-based energy dispersive X-ray diffraction (EDXRD) at the EDDI beamline of BESSY II at Helmholtz-Zentrum Berlin (HZB).[40] EDXRD spectra are recorded every 6 seconds by an energy-dispersive Ge detector with a diffraction angle of $2\theta = 6.26°$. The selenization conditions are identical to those described above. For more details see ref. 15.

UV-visible (UV-vis) spectrophotometry

The optically-derived (and thus *bulk*-sensitive) E_g values of the samples were obtained by means of ultraviolet-visible (UV-vis) spectrophotometry. Reflectance spectra were measured on a Perkin-Elmer Lambda 950 UV/Vis/NIR spectrophotometer.[41] Tungsten–halogen and deuterium lamps were used as excitation sources. The UV-vis portions of the spectra were detected *via* a photomultiplier. The near-infrared (NIR) portions of the spectra were recorded through a Peltier-cooled PbS detector setup. The measured reflectance spectra were evaluated by the Kubelka–Munk transformation method, in accordance to ref. 42. Assessment of the optical E_g was carried out by linear extrapolation of the leading edge of the transformed $(Kh\nu)^2$ *vs.* photon energy, $h\nu$, plots. Assuming an absorption coefficient (α) in the order of 10^4 cm^{-1} for photon energies just above the E_g (as reported for CISe[43]) of the samples, the information depth of this technique is estimated to be ~2 μm, which is in range of the thickness of the investigated chalcopyrite thin-films.[21]

Results and discussion

The X-ray photoelectron spectroscopy (XPS) survey spectrum of the KCN-etched CIS absorber (*cf.* ESI; Fig. S1† for more details) displays the photoemission and x-ray-excited Auger electron lines of the absorber elements (*i.e.*, Cu, In and S), as expected. Additional Se photoemission core levels appear in the survey spectra of all RTP-treated samples, even when Se is not intentionally supplied for the RTP process. [The deposited Se detected for sample (i) is ascribed to the background Se concentration in the RTP chamber.] At the same time, a reduction in the intensity of S-related core levels occurs in the spectra of RTP-treated samples. Traces of Na are detected in all RTP-treated samples, which are ascribed to an enhancement of Na diffusion from the Mo-coated SLG back contact induced by the high-temperature treatments.[44,45] Furthermore, the intensity of Cu-related photoemission lines increases in samples treated using longer periods and higher temperature ranges in the presence of Se vapor [*i.e.*, samples (v)–(vii)], suggesting an enrichment of surface Cu. These trends are better distinguished when examining detail XPS spectra in the Cu $2p_{3(1)/2}$, In $3d_{3/2}$, and S 2s/Se 3s regions (*cf.* ESI; Fig. S2† for more details). Additionally, *bulk* elemental analysis was conducted *via* X-ray fluorescence analysis (XRF), concentrating on the Cu K_α, In K_α, S K_α and Se K_α lines of the samples.

The (XPS-derived) surface and (XRF-derived) bulk [Se]/([S] + [Se]) ratios of the samples in the series are presented in Fig. 2, in ascending order of the determined surface value. The surface substitution of Se for S is observed for all samples undergoing RTP treatments. Changes in the bulk [Se]/([S] + [Se]) composition are only discerned in samples in which higher RTP temperatures and Se are used [*i.e.*, samples (iv)–(vii)]. These results show that it is possible to limit the effect of selenization treatment by careful selection of the employed RTP parameters. Within the set of samples with RTP-induced bulk modifications, samples (vi) and (vii) show slightly lower degrees of (surface and bulk) selenization. These variations are ascribed to the sealing limit of the graphite box (see Experimental Section). With higher temperature treatment, the leaking rate of Se vapor from the graphite box increases.[23]

The calculated values of the modified Se α^*, Cu α^* and In α^* are shown in Fig. 3a–c, as a function of surface [Se]/([S] + [Se]). Included in the figure are reported α^* ranges of values for reference compounds.[24,30,46–49] All RTP-treated samples show Se α^* values in the range reported for $CuInSe_2$ [within the margin of error for sample (iii), the sample with a surface [Se]/([S] + [Se]) ~ 0.48], as seen (black hollow squares) in Fig. 3(a). This fact indicates that Se incorporates into the chalcopyrite crystal lattice (Se_I) at the surface. However, the corresponding spectra (*cf.* ESI; Fig. S3† for more details) indicate for some samples the presence of a second Se species, and thus a secondary Se α^* (Se_{II}) was calculated [the red hollow circles in Fig. 3(a) are calculated by adding the BE of the Se $3d_{5/2}$ peak and the KE of the graphically derived Se LMM-like line of the Se_{II} component (*cf.* ESI; Fig. S3† for more details)]. For samples (i)–(iii), the secondary Se α^* values fall within the range of values reported for elemental Se, suggesting that the reaction conditions provided by the RTP-treatment parameters of samples in which elemental Se is detected are insufficient for the full incorporation of the reactant Se into the chalcopyrite alloy. Another possibility is that the elemental Se is deposited during the cool down period of the RTP process. The secondary Se α^* of sample (iv) – the sample with a surface [Se]/([S] + [Se]) of ~ 0.82 – is

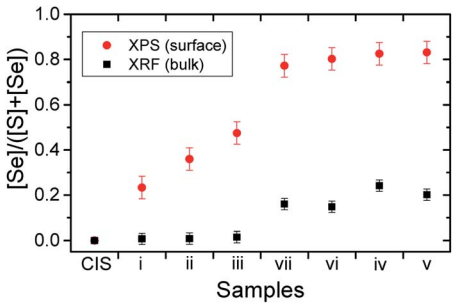

Fig. 2 Surface and bulk [Se]/([S] + [Se]) ratios obtained for the selenized CIS absorbers by XPS and XRF, respectively.

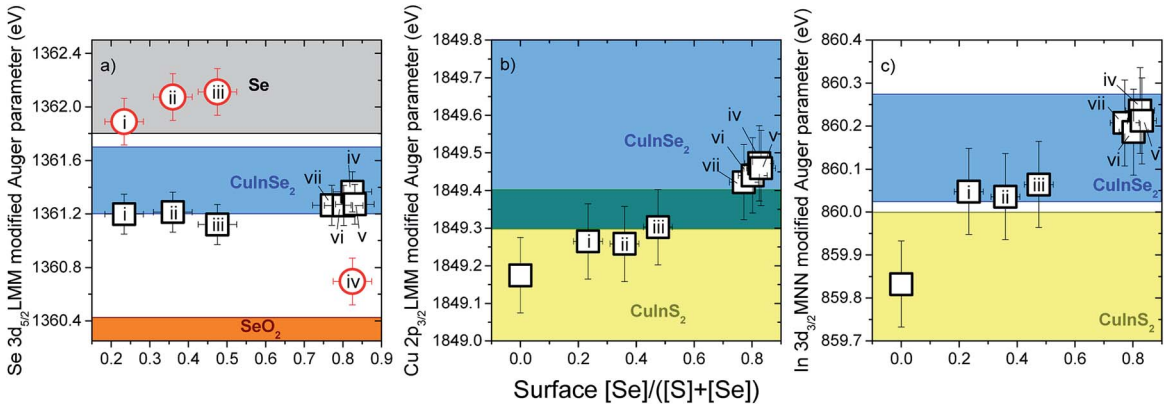

Fig. 3 Modified Auger parameters (α^*) for (a) Se, (b) Cu and (c) In of CIS and RTP-treated CIS absorbers, shown as a function of surface [Se]/([S] + [Se]). The shadowed areas correspond to α^* ranges for related reference compounds reported in literature.[24,30,46–49]

located close to the range of values reported for SeO_2; however, no signal is found near the BE ~59 eV region of its Se 3d XPS core level, expected for Se–O_x bonds.[24,30]

Fig. 3(b) shows the evolution of the Cu α^* values of the selenization series (*cf.* ESI; Fig. S4† for more details). A direct relation is found between the Cu α^* values of the samples and their surface [Se]/([S] + [Se]) composition. Although the Cu α^* values of the samples (i) and (ii) {*i.e.*, samples with surface [Se]/([S] + [Se]) ratios of 0.23 and 0.36, respectively} are still within the range of values reported for CIS, both values are close to the lower limit of the range of values reported for CISe. Samples with higher surface Se contents show Cu α^* values well within the range of values for CISe. Formation of $CuSe_2$ could not be excluded by this analysis due to overlapping Cu α^* values reported for Cu_2Se (1849.65 ± 0.15 eV)[24,30,46] and CISe (1849.55 ± 0.25 eV).[24,30,46]

The change in In α^* values of the samples as a function of surface [Se]/([S] + [Se]) composition is similar to that observed for the Cu α^* values (*cf.* ESI; Fig. S4† for more details), as shown in Fig. 3(c). The In α^* has also been reported to be an effective indicator of the degree of surface Cu-deficiency in CIS absorbers with Cu-richer CIS surfaces producing higher In α^* values compared to those obtained from Cu-poorer CIS surfaces.[49] In order to check whether the Cu-content of the studied sample set indeed varies, as suggested by the In α^* values, the surface composition is discussed below.

The surface compositions of the treated samples were quantified by correcting the intensities of the curve-fit-analyzed XPS core level peaks (*cf.* ESI; Fig. S2† for more details) by respective λ,[26,27] σ,[28] and T values.[29] Inclusion of surface Na in the quantification does not cause significant changes in the calculated surface compositions of the RTP-treated samples. Therefore, the Na surface content was omitted. Based on the evidence of the presence of elemental Se on the surface of the RTP-treated samples from the XAES analysis, the surface Se content of the samples was revised in order to obtain the actual chalcopyrite [Cu] : [In] : ([S] + [Se]) surface composition (*cf.* ESI; Fig. S3† for more details). For this purpose, a factor equivalent to the $Se_{II}/(Se_I + Se_{II})$ was subtracted from the Se 3s intensity used for the surface composition quantification. {The corrected anion composition ratio is denoted as "surface chalcopyrite [Se]/([S] + [Se])" in figures below}. The obtained [Cu] : [In] : ([S] + [Se]) compositions are shown in Fig. 4.

The untreated CIS absorber shows a Cu-poor, In-rich surface, slightly deviating from the [Cu] : [In] : [S] = 1 : 3 : 5 stoichiometry. An explanation for this deviation in surface composition may be an incomplete removal of the $Cu_{2-x}S$ cap by the KCN etching.[21,22] In contrast, XRF measurements of the (KCN-treated) CIS absorber yield Cu and In elemental fractions of 0.25 and 0.28, respectively, thus indicating Cu and In near stoichiometric compositions in the bulk. As shown in Fig. 4, the RTP selenization treatment does not only incorporate Se into the CIS absorber but also induces changes in the cation content at the absorber surface. At first, the incorporation of Se appears to decrease the surface concentration of Cu, while leaving the surface concentration of In relatively unchanged. This trend continues up to sample (iii) {*i.e.*, the sample with a surface chalcopyrite [Se]/([S] + [Se]) ~ 0.43}, which exhibits a surface that is in close agreement with a [Cu] : [In] : ([S] + [Se]) = 1 : 3 : 5 stoichiometry. Further surface selenization induces a surface Cu-enrichment, along with a decrease in the initial surface In content of the CIS absorber. As a result, the initial Cu-poor surface of the CIS

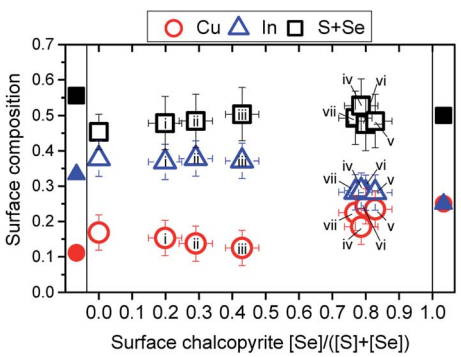

Fig. 4 XPS-determined surface composition of CIS and RTP-treated CIS absorbers, shown as a function of surface chalcopyrite [Se]/([S] + [Se]). The solid icons at the left and right margins represent 1 : 3 : 5 and 1 : 1 : 2 Cu : In : (S + Se) stoichiometries, respectively.

absorber is converted into a Cu-richer [Cu] : [In] : ([S] + [Se]) = 1 : 1 : 2 type stoichiometry.

In any case, samples with a lower Se surface content show Cu-poor, In-rich surface compositions. Theoretical work proposes that the presence of electrically neutral defect pairs is possible in chalcopyrite surfaces of similar compositions due to relatively low formation energies for Cu vacancies.[50] More specifically, two Cu vacancy sites (acceptor states), V_{Cu}^{-}, couple with an In atom occupying a copper site (donor states), In_{Cu}^{++} (*i.e.*, 2 V_{Cu}^{-} + In_{Cu}^{++}). In the present case, however, the chalcopyrite anion content is lower than expected for a surface [Cu] : [In] : ([S] + [Se]) = 1 : 3 : 5 composition, which suggests S site vacancies, *i.e.* V_S^{++}. The deposition of Se seems to fill these V_S^{++}. With further incorporation of Se into the absorber surface, the Cu surface concentration decreases, as seen for samples (i)–(iii) {samples with a surface chalcopyrite [Se]/([S] + [Se]) range ~0.2–0.4}, suggesting a greater formation of V_{Cu}^{-} sites. Although a proportional formation of In_{Cu}^{++} would be needed to compensate for the new V_{Cu}^{-}, the In surface concentration remains unchanged for these samples, indicating no increase in In_{Cu}^{++}. This missing compensation in charged defect pairing can be due to higher energies of formation of In_{Cu}^{++} antisites compared to V_{Cu}^{-} sites in Cu-poor, In-rich chalcopyrite lattices, as predicted by theoretical models.[50]

An alternative charge pairing mechanism driven by the deposited Se and the conversion of V_{Cu}^{-} to V_{Cu}^{0} is proposed in the following. Incorporation of Se into the chalcopyrite matrix entails a reduction process of the deposited elemental Se (Se^0) into a chalcopyrite Se anion (Se^-) (*i.e.*, $Se^0 + 2e^- \rightarrow Se^-$). Moreover, low formation energies for single neutral defects (more specifically, V_{Cu}^{0}) are also reported in Cu-poor CISe surfaces.[50] The Cu depletion (*i.e.*, increased formation of V_{Cu} sites) observed in samples (ii) and (iii) stands out as a potential source of electrons for the reduction of Se^0 (*i.e.*, $Se^0 + 2V_{Cu}^{-} \rightarrow Se^0 + 2V_{Cu}^{0} + 2e^- \rightarrow Se^- + 2V_{Cu}^{0}$). The energy requirements for the formation of both V_{Cu}^{-} and V_{Cu}^{0} increase as the VBM of the chalcopyrite shifts closer to the E_F level. Because the substitution of S by Se moves the VBM of the RTP-treated samples towards the E_F level (discussed below), V_{Cu}^{-} and V_{Cu}^{0} sites in samples with higher surface Se content [samples (iv)–(vi)] become energetically unfavorable.[50,51] As presented in Fig. 4, these samples undergo a surface Cu-enrichment, which leads to a surface composition transition from [Cu] : [In] : ([S] + [Se]) ~ 1 : 3 : 5 to [Cu] : [In] : ([S] + [Se]) = 1 : 1 : 2. Although thermally-mediated Cu diffusion mechanisms have been reported for heterointerfaces with elemental compositions similar to the RTP-treated CIS samples (*e.g.*, In_2S_3/CIGSe),[52,53] the Cu-enrichment observed for the set of RTP-treated CIS samples with higher surface Se content [samples (iv)–(vi)] does not seem to be induced by the heat of the process. Otherwise, all RTP-treated samples should show signs of surface Cu-enrichment: the 300–550 °C temperature range used in the RTP treatments is significantly higher than the 200 °C annealing temperature reported to induce Cu-diffusion across the In_2S_3/CIGSe heterointerface.[52,53] Moreover, the treatment of the RTP control sample [*i.e.*, sample (i), which shows no signs of surface Cu-enrichment] uses the same treatment temperature and duration as the treatment for sample (vi), which shows a surface Cu-enrichment. A threshold for the Se composition, which controls the energetic distance of the VBM to the E_F level, seems to activate the observed Cu-diffusion from the bulk to the surface of the samples.

UPS was used to measure the position of the VBM with respect to the E_F level of the samples (*cf.* ESI; Fig. S5† for more details). The VBM of all RTP-treated samples shifts closer to the E_F level [from (−0.88 ± 0.08) eV for CIS to (−0.51 ± 0.08) eV for sample (vii)] upon incorporation of Se in the surface of the samples. Based on the surface composition results discussed above, V_{Cu} sites are expected to form in samples with a VBM lower boundary down to ~−0.7 eV [samples (i)–(iii)]. This lower limit in the distance between the VBM and the E_F level is slightly lower (by ~0.1 eV) than the ones reported in a previous work.[51] Nonetheless, the measured VBM levels of samples undergoing surface Cu-enrichment (*i.e.*, ~−0.55 eV) are consistent with the E_F-level dependence of the formation of Cu-related defects in chalcopyrite absorbers.[50,51]

Optically derived E_g values of ~1.47 eV are found for the CIS absorber and for RTP-treated samples with low surface Se contents (*cf.* ESI; Fig. S6† for more details), indicating that the selenization is limited to the near-surface region of the absorbers. These observed optical E_g values are slightly lower than the bulk E_g value of CIS (*i.e.*, 1.54 eV).[20] Similar slightly reduced optical E_g values of CIS absorbers have been reported and are ascribed to absorption/reflectance losses due to surface roughness and/or deviations of stoichiometric compositions.[54] Because the CIS absorbers were produced by RTP, a rough absorber morphology can be expected.[21] Moreover, the XRF measurements of the CIS absorber yield a stoichiometric Cu (0.25) and slightly S-poor (0.47) bulk composition, which has been shown to reduce the optical E_g to the observed values.[54] Lower optical E_g values (*i.e.*, 1.06–1.14 eV), which fall within range of optical E_g values of CISe,[9] are measured for samples with higher degrees of selenization (*cf.* ESI; Fig. S6† for more details). These findings suggest that the RTP-parameters used for the treatments of samples with higher surface chalcopyrite [Se]/([S] + [Se]) ratios increase the treatment effect depth, as the electronic, chemical and optical properties inside the bulk of the samples. These observations are in agreement with the formation of a $CuIn(S,Se)_2$ (CISSe) phase on top of a remaining pure CIS layer, confirmed by energy dispersive X-ray diffraction (EDXRD) measurements shown in Fig. 5. The figure shows that the CIS 112 diffraction signal only decreases in intensity, but does not shift due to Se incorporation (a slight shift to lower energies can be explained by thermal expansion). A broader signal between the expected positions of CIS 112 and CISe 112 reveals formation of CISSe. However, this CIS → CISSe conversion strongly depends on the RTP process parameters. Thus, a common re-sulfurization of the surface[55–57] is expected to result in a notch-type band gap grading (*i.e.*, high absorber band gap energies toward the back contact and the surface) that proved to result in the highest power conversion efficiencies in the past if induced by an x = [Ga]/([In] + [Ga]) ratio grading.[12]

Fig. 6 combines the observed changes in electronic and optical properties of the sample series. An assessment of

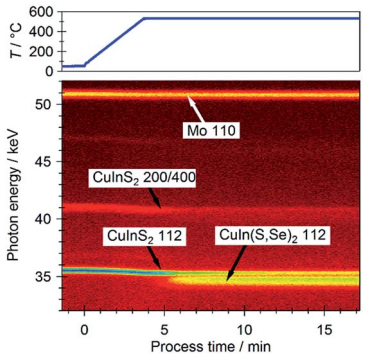

Fig. 5 Real-time X-ray diffraction data recorded during the selenization of a CIS film at 530 °C with 5 mg Se. The top part shows the temperature measured by a thermocouple placed above the sample. The bottom part shows color-coded EDXRD intensities *vs.* photon energy and annealing time. The intensities increase from dark red to blue.

changes in the surface band gap, E_g^{surf}, of the samples is pursued. The hollow black squares show the surface VBM position of the samples in the series as a function of surface chalcopyrite [Se]/([S] + [Se]), as determined by the UPS analysis (*cf.* ESI; Fig. S5† for more details). By adding the optical (bulk) E_g^{bulk} value (*cf.* ESI; Fig. S6† for more details) to the VBM value of the corresponding sample, an estimation of the CBM of each sample (*i.e.*, CBM = VBM + E_g^{bulk}, hollow red circles) is presented. For this assessment to be valid, the chemical structures of the bulk and the surface of the sample have to be the same. Included in Fig. 6 are CBM and VBM values of chalcopyrite absorbers determined by inverse photoemission spectroscopy (IPES) and UPS measurements, respectively, reported in ref. 31–36. {Note that, except for values from ref. 33, all reference values were measured from chalcopyrites reported to exhibit Cu-poor surfaces. Moreover, the Cu(In,Ga)S_2 (CIGS) absorber of ref. 32 was reported to be Ga-depleted at the surface, rendering it CIS-like.} Because the surface elemental compositions of CIS

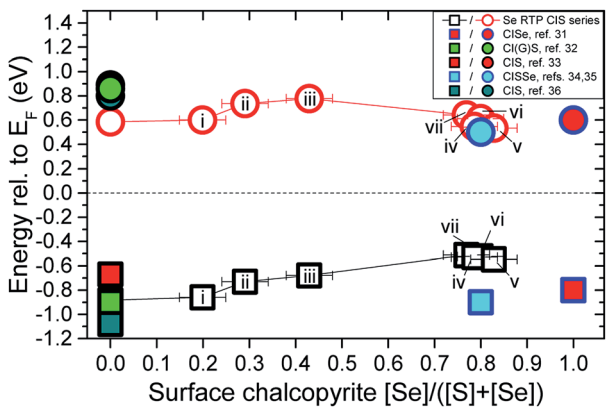

Fig. 6 Changes in VBM position (hollow black squares) and estimated CBM values (*i.e.*, calculated CBM = VBM + E_g^{bulk}, hollow red circles) of the investigated RTP-treated sample series as a function of the surface chalcopyrite [Se]/([S] + [Se]) composition. Included are CBM and VBM values of chalcopyrite absorbers determined by IPES and UPS measurements, reported in ref. 31–36.

absorbers and the RTP-treated samples (i)–(iii) {samples with [Se]/([S] + [Se]) < 0.5} were found to be Cu-poor, an enlarged E_g^{surf} (relative to the bulk) can be expected at the surface compared to the bulk in these samples. A comparison between the reported (measured) CBM values of CI(G)S absorbers and the calculated CBM values of the KCN-etched CIS and the RTP-treated samples (i)–(iii) of the investigated series shows a significant difference, highlighting this surface band gap widening. Therefore, we can expect the mean of the reference CBM values (0.85 ± 0.1 eV) to better represent the upper limit of the CBM of the Cu-poor samples in the series. It is not possible to conclude whether the shifting of the VBM values closer to the E_F level can be ascribed solely to a reduction of the E_g^{surf} (due to a higher Se surface content) or whether a shifting of both, the CBM and the VBM, takes place due to changes in doping level as a function of surface [Se]/([S] + [Se]). In the latter case, CBM values of the RTP-treated samples could be greater than the assumed 0.85 eV upper boundary.

Samples with surface chalcopyrite [Se]/([S] + [Se]) > 0.5 eV [*i.e.*, samples (iv)–(vii)] exhibit more uniform 1 : 1 : 2 compositions at the surface and in the bulk. Therefore, the approach taken to estimate the CBM value of these samples (*i.e.*, adding the optical E_g value to the VBM value of the sample) is certainly more valid and in good agreement with CBM values reported for CI(S)Se absorbers.[31,34,35] However, for these samples a significant difference is found at the VBM position, which is significantly closer to the E_F level than for CI(S)Se absorbers reported in ref. 31, 34 and 35. This difference can be explained by the loss of surface Cu-deficiency for this subset of the RTP-treated samples, which results in the appearance of p–d repulsions between the valence states of the chalcopyrite anions (S 3p and Se 4p) and the Cu 3d derived orbitals that pushes the VBM closer to the E_F level.[58] The lower CBM values calculated for these samples suggest that the modified absorber surfaces may be better suited for the formation of potentially optimized buffer/absorber band alignments with CdS [*i.e.*, the mean CBM value of (directly measured) CdS on Se-containing chalcopyrite absorbers is 0.56 ± 0.17 eV].[31,34–36,59,60] However, the VBM shift toward the E_F level at the surface of the absorber is expected to increase the hole density at the interface, leading to an increase in recombination losses ultimately affecting the performance (*i.e.*, open circuit voltage, V_{OC}) of produced solar cell devices. A potential route to overcome this obstacle would be to use Cu-poorer CIS substrates to limit the enrichment of Cu at the surface induced by the RTP selenization treatments. Moreover, subsequently widening the E_g^{surf} (*e.g.*, by way of surface sulfurization) of a bulk-selenized RTP treated sample [*e.g.*, samples (iv)–(vi)] could lead to the production of an absorber with a wide front side E_g/low bulk E_g/wide back side E_g configuration (see discussion above). The following device performance benefits would be expected from such configuration: (i) a wide E_g at the front side would increase the interface band gap and decrease recombination losses at the buffer/absorber interface;[61] (ii) a wide E_g at the back side would act as a "mirror" for electrons and prevent recombination losses at the absorber/back contact interface;[62] (iii) an optimized E_g minimum at the bulk would allow for high photon absorption, as well as, high V_{OC} outputs.[12]

Conclusions

In summary, an RTP-based treatment to incorporate Se into the surface of CIS absorbers was presented. A substitution of S by Se takes place as a result of all RTP treatments. The VBM shifts towards the E_F level and a reduction of the optical E_g can be observed. Both observations are in agreement with the formation of a CISSe phase *on top* of the treated CIS substrate, which is confirmed through EDXRD. This CIS → CISSe conversion {*i.e.*, its [Se]/([S] + [Se]) ratio} and the effective depth of the treatment strongly depend on the RTP process parameters. In samples with higher selenization, the initially Cu-poor CIS surface changes to a surface with a stoichiometric Cu : In : (S + Se) = 1 : 1 : 2 composition. Additional surface treatments (*e.g.*, surface sulfurization) will be required to achieve the desirable notch-type band gap grading, currently resulting in the higher power conversion efficiencies. The presence of elemental Se is also detected in all treated samples; its removal is needed (*e.g.*, by a post-RTP annealing treatment)[63] to prevent it from limiting the performance of solar cell devices based on RTP-treated CIS absorbers.

Conflicts of interest

There are no conflicts to declare.

Acknowledgements

This work was supported in part by the Helmholtz-Association (VH-NG-423). R. F. is also grateful to the German Academic Exchange Agency (DAAD; 331 4 04 002) for financial support. We thank HZB for the allocation of synchrotron radiation beamtime.

References

1 Press Release: Solar Frontier Achieves World Record Thin-Film Solar Cell Efficiency of 22.9%, Tokyo, December 20, 2017, http://www.solar-frontier.com/eng/news/2017/1220_press.html.
2 P. Jackson, R. Wuerz, D. Hariskos, E. Lotter, W. Witte and M. Powalla, *Phys. Status Solidi RRL*, 2016, **10**, 583.
3 P. Jackson, D. Hariskos, R. Wuerz, O. Kiowski, A. Bauer, T. M. Friedlmeier and M. Powalla, *Phys. Status Solidi RRL*, 2015, **9**, 28.
4 P. Jackson, D. Hariskos, R. Wuerz, W. Wischmann and M. Powalla, *Phys. Status Solidi RRL*, 2014, **8**, 219.
5 A. Chirilă, P. Reinhard, F. Pianezzi, P. Bloesch, A. R. Uhl, C. Fella, L. Kranz, D. Keller, C. Gretener, H. Hagendorfer, D. Jaeger, R. Erni, S. Nishiwaki, S. Buecheler and A. N. Tiwari, *Nat. Mater.*, 2013, **12**, 1107.
6 L. Stolt, presented at *IWG-CIGSTech 5 Solibro CIGS to the next level*, Berlin, Germany, April 2014.
7 K. Kushia, presented at *IWG-CIGSTech 5 Current Status and Future Prospects of Solar Frontier*, Berlin, Germany, April 2014.
8 P. Jackson, D. Hariskos, E. Lotter, S. Paetel, R. Wuerz, R. Menner, W. Wischmann and M. Powalla, *Prog. Photovoltaics Res. Appl.*, 2011, **19**, 894.
9 M. Bär, W. Bohne, J. Röhrich, E. Strub, S. Lindner, M. C. Lux-Steiner, C.-H. Fischer, T. P. Niesen and F. Karg, *J. Appl. Phys.*, 2004, **96**, 3857.
10 L. L. Kazmerski, *Technical Digest of the 12th International Photovoltaic Science and Engineering Conference: PVSEC-12*, Jeju, South Korea, 2001, p. 11.
11 W. Shockley and H. J. Queisser, *J. Appl. Phys.*, 1961, **32**, 510.
12 A. Chirilă, S. Buecheler, F. Pianezzi, P. Bloesch, C. Gretener, A. R. Uhl, C. Fella, L. Kranz, J. Perrenoud, S. Seyrling, R. Verma, S. Nishiwaki, Y. E. Romanyuk, G. Bilger and A. N. Tiwari, *Nat. Mater.*, 2011, **10**, 857.
13 M. Marudachalam, R. W. Birkmire, H. Hichri, J. M. Schultz, A. Swartzlander and M. M. Al-Jassim, *J. Appl. Phys.*, 1997, **82**, 2896.
14 M. Marudachalam, H. Hichri, R. Klenk, R. W. Birkmire, W. N. Shafarman and J. M. Schultz, *Appl. Phys. Lett.*, 1995, **67**, 3978.
15 R. Mainz, A. Weber, H. Rodriguez-Alvarez, S. Levcencu, M. Klaus, P. Pistor, R. Klenk and H.-W. Schock, *Prog. Photovoltaics Res. Appl.*, 2015, **23**, 1131.
16 S. S. Schmidt, C. Wolf, H. Rodriguez-Alvarez, C. A. Kaufmann, J.-P. Bäcker, M. Hartig, S. Merdes, F. Ziem, I. Dorbandt, C. Köble, S. Cinque, D. Abou-Ras, R. Mainz and R. Schlatmann, *Prog. Photovoltaics Res. Appl.*, 2017, **25**, 341.
17 J. Palm, V. Probst, W. Stetter, R. Toelle, S. Visbeck, H. Calwer, T. Niesen, H. Vogt, O. Hernández, M. Wendl and F. H. Karg, *Thin Solid Films*, 2004, **451–452**, 544.
18 R. Caballero, C. Guillén and C. A. Kaufmann, *Prog. Photovoltaics Res. Appl.*, 2006, **14**, 145.
19 W.-C. Hsu, B. Bob, W. Yang, C.-H. Chung and Y. Yang, *Energy Environ. Sci.*, 2012, **5**, 8564.
20 H. Landolt, R. Börnstein, K. H. Hellwege, M. Böhn, M. S. H. Weiss and O. Madelung, in *Landolt-Börnstein Numerical Data and Functional Relationships in Science and Technology. Group 3, Crystal and Solid State Physics*, ed. O. Madelung, M. Schulz and H. Weiss, Springer, Berlin, Germany, 1985, vol. 17.
21 K. Siemer, J. Klaer, I. Luck, J. Bruns, R. Klenk and D. Bräunig, *Sol. Energy Mater. Sol. Cells*, 2001, **67**, 159.
22 M. Weber, R. Scheer, H. J. Lewerenz, H. Jungblut and U. Störkel, *J. Electrochem. Soc.*, 2002, **149**, G77.
23 H. Rodriguez-Alvarez, PhD thesis, Technische Universität Berlin, Berlin, Germany, February 2010.
24 In *Practical Surface Analysis: Auger and X-ray Photoelectron Spectroscopy*, ed. D. Briggs and M. P. Frye, Wiley, New York, NY, USA, 1983.
25 M. Wojdyr, *J. Appl. Crystallogr.*, 2010, **43**, 1126.
26 S. Tougaard, *QUASES-IMFP-TPP2M*, 2002.
27 S. Tanuma, C. J. Powell and D. R. Penn, *Surf. Interface Anal.*, 1994, **21**, 165.
28 M. B. Trzhaskovskaya, V. I. Nefedov and V. G. Yarzhemsky, *At. Data Nucl. Data Tables*, 2001, **77**, 97.

29 M. P. Seah and G. C. Smith, *Surf. Interface Anal.*, 1990, **15**, 751.
30 J. F. Moulder, W. F. Stickle, P. E. Sobol and K. D. Bomben, in *Handbook of X-ray Photoelectron Spectroscopy: A Reference Book of Standard Spectra for Identification and Interpretation of XPS Data*, ed. J. Chastain and R. C. King Jr, Perkin-Elmer, Physical Electronics Division, Eden Prairie, MN, USA, 2nd edn, 1995.
31 M. Morkel, L. Weinhardt, B. Lohmüller, C. Heske, E. Umbach, W. Riedl, S. Zweigart and F. Karg, *Appl. Phys. Lett.*, 2001, **79**, 4482.
32 L. Weinhardt, O. Fuchs, D. Groß, G. Storch, E. Umbach, N. G. Dhere, A. A. Kadam, S. S. Kulkarni and C. Heske, *Appl. Phys. Lett.*, 2005, **86**, 062109.
33 M. Bär, J. Klaer, L. Weinhardt, R. G. Wilks, S. Krause, M. Blum, W. Yang, C. Heske and H.-W. Schock, *Adv. Energy Mater.*, 2013, **3**, 777.
34 M. Bär, PhD thesis, Technische Universität Berlin, Berlin, Germany, December 2003.
35 L. Weinhardt, PhD thesis, Bayerische Julius-Maximilians-Universität, Würzburg, Germany, December 2005.
36 R. Félix-Duarte, PhD thesis, Brandenburgische Technische Universität, Cottbus, Germany, April 2015.
37 M. P. Seah and W. A. Dench, *Surf. Interface Anal.*, 1979, **1**, 2.
38 X-ray Fluorescence Spectrometer ZSX Primus II, *Rigaku J.*, 2005, **22**, 42.
39 B. L. Henke, E. M. Gullikson and J. C. David, *At. Data Nucl. Data Tables*, 1993, **54**, 181.
40 C. Genzel, I. A. Denks, R. Coelho, D. Thomas, R. Mainz, D. Apel and M. Klaus, *J. Strain Anal. Eng. Des.*, 2011, **46**, 615.
41 LAMBDA 950 UV/Vis Spectrophotometer, http://www.perkinelmer.com/product/lambda-950-uv-vis-nir-spectrophotometer-l950.
42 P. Kubelka, *J. Opt. Soc. Am.*, 1958, **38**, 448.
43 W. Hörig, H. Neumann, H. Sobotta, B. Schumann and G. Kohn, *Thin Solid Films*, 1978, **48**, 67.
44 D. Schmid, M. Ruckh, F. Grunwald and H.-W. Schock, *J. Appl. Phys.*, 1993, **73**, 2902.
45 D. Schmid, M. Ruckh and H.-W. Schock, *Sol. Energy Mater. Sol. Cells*, 1996, **41–42**, 281.
46 E. Niemi and L. Stolt, *Surf. Interface Anal.*, 1990, **15**, 422.
47 R. Scheer and H. J. Lewerenz, *J. Vac. Sci. Technol., A*, 1994, **12**, 56.
48 S. Andres, C. Lehmann and C. Pettenkofer, *Thin Solid Films*, 2009, **518**, 1032.
49 M. Bär, J. Klaer, R. Félix, N. Barreau, L. Weinhardt, R. G. Wilks, C. Heske and H.-W. Schock, *IEEE J. Photovolt.*, 2013, **3**, 828.
50 S. B. Zhang, S.-H. Wei, A. Zunger and H. Katayama-Yoshida, *Phys. Rev. B: Condens. Matter Mater. Phys.*, 1998, **57**, 9642.
51 A. Klein and W. Jaegermann, *Appl. Phys. Lett.*, 1999, **74**, 508.
52 P. Pistor, N. Allsop, W. Braun, R. Caballero, C. Camus, C.-H. Fischer, M. Gorgoi, A. Grimm, B. Johnson, T. Kropp, I. Lauermann, H. Mönig, S. Schorr, A. Weber and R. Klenk, *Phys. Status Solidi A*, 2009, **206**, 1059.
53 M. Bär, N. Barreau, F. Couzinié-Devy, S. Pookpanratana, J. Klaer, M. Blum, Y. Zhang, W. Yang, J. D. Denlinger, H.-W. Schock, L. Weinhardt, J. Kessler and C. Heske, *Appl. Phys. Lett.*, 2010, **96**, 184101.
54 N. Guezmir, J. Ouerfelli and S. Belgacem, *Mater. Chem. Phys.*, 2006, **96**, 116.
55 T. Nakada, H. Ohbo, T. Watanabe, H. Nakazawa, M. Matsui and A. Kunioka, *Sol. Energy Mater. Sol. Cells*, 1997, **49**, 285.
56 D. Ohashi, T. Nakada and A. Kunioka, *Sol. Energy Mater. Sol. Cells*, 2001, **67**, 261.
57 T. Kobayashi, H. Yamaguchi, Z. J. Li Kao, H. Sugimoto, T. Kato, H. Hakuma and T. Nakada, *Prog. Photovoltaics Res. Appl.*, 2015, **23**, 1367.
58 J. E. Jaffe and A. Zunger, *Phys. Rev. B: Condens. Matter Mater. Phys.*, 1984, **29**, 1882.
59 D. Hauschild, D. Kreikemeyer-Lorenzo, P. Jackson, T. Magorian Friedlmeier, D. Hariskos, F. Reinert, M. Powalla, C. Heske and L. Weinhardt, *ACS Energy Lett.*, 2017, **2**, 2383.
60 S. Pookpanratana, PhD thesis, University of Nevada, Las Vegas, Las Vegas, USA, December 2010.
61 R. Scheer, *J. Appl. Phys.*, 2009, **105**, 104505.
62 M. Bär, S. Nishimaki, L. Weinhardt, S. Pookpanratana, W. N. Shafarman and C. Heske, *Appl. Phys. Lett.*, 2008, **93**, 042110.
63 R. Hunger, T. Schulmeyer, A. Klein, W. Jaegermann, K. Sakurai, A. Yamada, P. Fons, K. Matsubara and S. Niki, *Surf. Sci.*, 2004, **557**, 263.